

Protein Fibrillar Nanopolymers: Molecular-Level Insights into Their Structural, Physical and Mechanical Properties

Valeriya M. Trusova

*Department of Nuclear and Medical Physics
V. N. Karazin Kharkiv National University
4 Svobody Sq. Kharkiv 61072, Ukraine
valtrusova@yahoo.com*

Received 10 March 2015

Revised 1 June 2015

Accepted 17 June 2015

Published 1 September 2015

Amyloid fibrils represent a generic class of mechanically strong and stable biomaterials with extremely advantageous properties. Although amyloids were initially associated only with severe neurological disorders, the role of these structures nowadays is shifting from health debilitating to highly beneficial both in biomedical and technological aspects. Intensive involvement of fibrillar assemblies into the wide range of pathogenic and functional processes strongly necessitate the molecular level characterization of the structural, physical and elastic features of protein nanofibrils. In the present contribution, we made an attempt to highlight the up-to-date progress in the understanding of amyloid properties from the polymer physics standpoint. The fundamental insights into protein fibril behavior are essential not only for development of therapeutic strategies to combat the protein misfolding disorders but also for rational and precise design of novel biodegradable protein-based nanopolymers.

Keywords: Amyloid fibrils; biopolymers; structure-property relationship; polymorphism; models of formation.

1. Introduction

A diverse collection of peptides and proteins has the unique propensity to self-assemble into insoluble fibrous quaternary structure enriched in intermolecularly hydrogen bonded β -sheets.^{1–3} Initially introduced by Virchow in 1854, the term “amyloid” has been used to describe specific macroscopic abnormal formulations deposited extra- or intra-cellularly and consisting primarily of polysaccharide or proteinaceous components.⁴ Lately, in a search of its more strict definition, this term has been subjected to long scientific debates. Finally, three main criteria have been emerged to identify amyloid structures: (i) Amyloid should possess specific tinctorial properties, i.e., apple green birefringence under cross-polarized light upon

staining with histological dye Congo red,⁵ (ii) in the electron microscopy images amyloids should be visualized as uniform structurally rigid fibrils with average diameter ~ 10 nm⁶ and (iii) X-ray diffraction patterns of amyloids should yield repeated cross- β structure, in which β -strands run perpendicularly to the long axis of the fibril, while β -sheets propagate in its direction.^{7,8}

Originally, amyloid fibrils were associated with a wide range of debilitating disorders, including Parkinson's, Alzheimer's, Huntington's, Creutzfeld–Jakob diseases, type II diabetes, bovine spongiform encephalopathy, etc. A diversity of hypotheses regarding the amyloid cytotoxicity has been suggested involving activation of signal pathways,⁹ generation of reactive oxygen species,¹⁰ binding of cellular proteins,¹¹ interaction with cell receptors,¹² disruption of biological membranes,^{13,14} just to name a few. Along with pathogenic protein fibrillar aggregates, so-called “functional amyloids” have been discovered.^{2,15,16} These protein assemblies possess structural and physicochemical properties that allow them to be classified as amyloid, but their physiological properties are functional rather than disease-related. The examples embrace human melanosomes,¹⁷ curli protein and inclusion bodies,¹⁶ bacterial coatings,¹⁸ catalytic scaffolds,¹⁹ adhesives,²⁰ structures for the storage of peptide hormones,²¹ etc. Furthermore, superior physical properties of amyloids, such as high mechanical strength, stiffness, rigidity, thermal stability, elongated morphology with highly hierarchical order, open up new horizons in creation of novel functional bionanomaterials for various applications ranging from biotechnology to nanoelectronics. Several examples may include the use of protein fibrils as a depot for drug transport,²² scaffolds in tissue bioengineering,²³ for construction of metallic nanowires²⁴ and self-assembled nanostructures,²⁵ and as functional templates.²⁴ These findings shifted the accent in amyloid interpretation from medical framework to soft condensed matter description, according to which protein fibrils are considered as semiflexible biopolymers obeying basic physical laws.²⁶ This approach turned out to be more appropriate since molecular level understanding of physical properties of protein nanoassemblies is of utmost necessity both for antagonizing the conformational disorders as well as for smart design of novel functional materials. In the given contribution, we attempted to highlight the progress in the field of amyloid physics based on the overview of available information. We will discuss key questions related to the molecular architecture and structural polymorphism of the fibrillar aggregates, their elastic and physicochemical properties. Finally, we will give a brief look at the phase behavior of protein fibrils in aqueous solution.

2. Structure and Formation of Amyloid Fibrils

A diversity of experimental techniques, such as X-ray diffraction, solid-state NMR, EPR, AFM, cryo-electron and electron microscopy, have been employed to decipher the ultrastructural organization of amyloid fibrils.²⁷ These analytical tools revealed a clear structural hierarchy of protein fibrillar aggregates. Secondary structure is dominated by β -strands and disordered regions (loops and bends). At the level

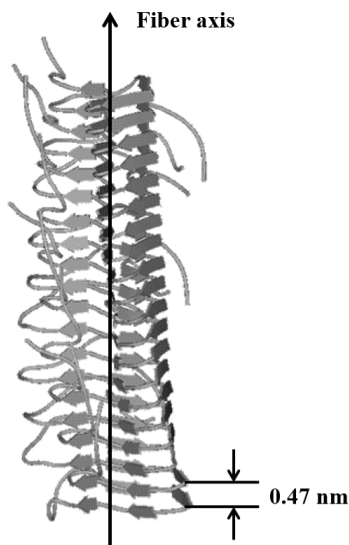


Fig. 1. Schematic representation of β -sheet arrangement in amyloid fibril core.

of tertiary structure, β -strands are packed into continuous parallel or antiparallel hydrogen-bonded β -sheets.² In such organization, β -strands are separated by $\sim 4.7 \text{ \AA}$ and extend orthogonally to the fibril axis. Clustering of β -sheets parallel to the long axis of the fibril determines the quaternary structure of the protein self-assemblies. The intersheet separation distance is about 9–11 \AA .^{28,29} The foregoing architecture is called a cross- β structure and represents the molecular level fingerprint of each protofilament (Fig. 1).

More comprehensive description of amyloid structure may be replenished by the cross- β spine steric zipper model suggesting that two β -sheets may form the U-turn. In this configuration, the β -strands of the opposing sheets are slightly offset relative to each other so that side chains from one sheet interdigitate in between the side chains of another sheet.³⁰ The interface between two adjacent β -sheets is completely excluded from water (so-called “dry interface”).³¹ This self-complementary steric zipper is stabilized mainly by van der Waals and hydrophobic interactions and is repeated along the entire length of the fibril.

Generally, the protein fibrillization is recognized as clearly defined nucleation–elongation process, occurring via primary homogeneous nucleation mechanism (Fig. 2).

According to nucleation-dependent model, the aggregation begins with clustering of monomeric species into the nucleus which subsequently grows through the monomer addition, eventually resulting in the formation of protofibrils or protofilaments. This sequence of events manifests itself in characteristic sigmoidal kinetic profile for the increase of mass-in-aggregate (Fig. 3).

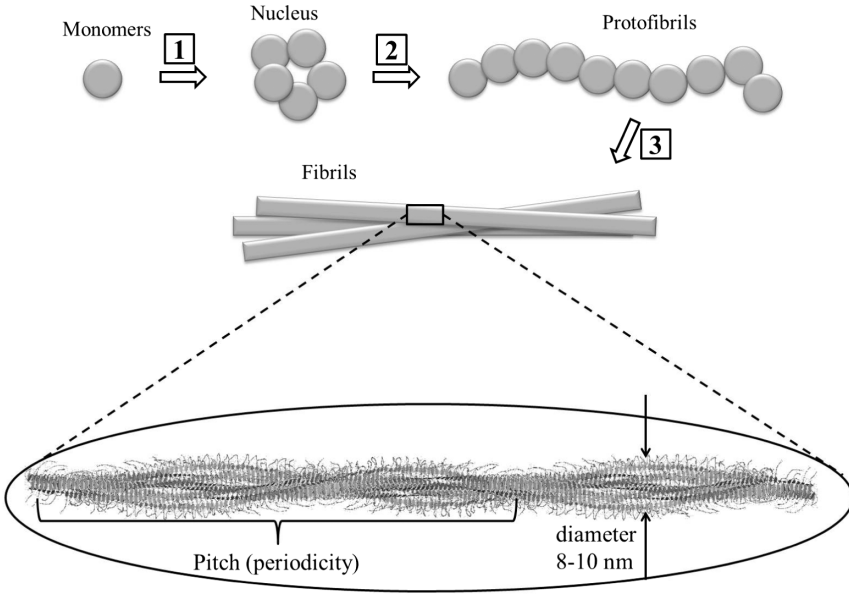


Fig. 2. Simplified illustrative scheme of nucleation-dependent polymerization model. Grey circle represents protein monomer.

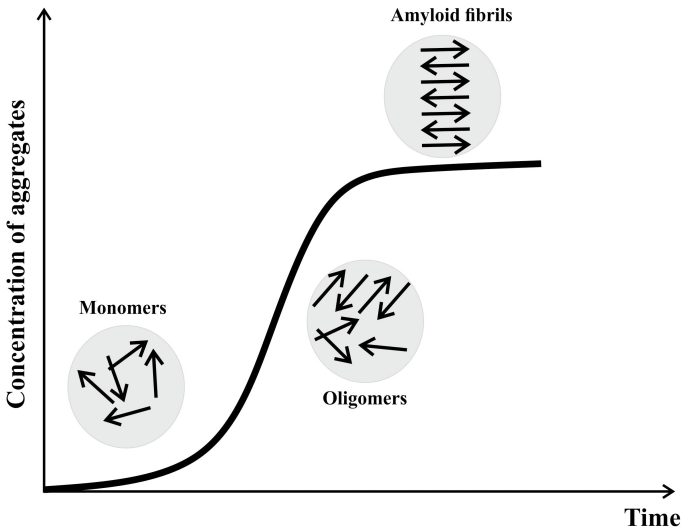


Fig. 3. Kinetic profile of amyloid fibril growth according to primary nucleation concept.

In the present context, it is of utmost importance to mention that according to the prevailing hypothesis, only monomers are present in the lag phase, as shown simplistically in Fig. 3. However, very recent studies indicate that primary nuclei formed during the lag phase may compete with the nuclei formed via secondary nucleation reactions which are catalyzed by the surface of the fibrils.^{32–34}

Since the rate constant for fibril growth is much higher than that for the nucleus generation, the first formed fibrils may be present in solution soon after the formation of the first nuclei. These fibrils are thought to represent the template for secondary nucleation event. In other words, aggregation process is characterized by nonlinearity manifesting itself in simultaneous realization both of primary and secondary nucleation pathways during the lag period. This means that some fraction of fibrillary structures may appear already during this phase. According to secondary nucleation mechanism, further amyloid growth occurs via sequential monomer addition, i.e. attachment of the monomer to the sides of the protofilaments. Although this concept is currently acquiring its experimental and theoretical support,^{32,35} the basic fibrillization route assumes that concentration fluctuations result in increasing local density of individual protofilaments due to their close approaching.^{36,37} This mediates the inter-protofilament interactions followed by protofilament irreversible aggregation and intertwining along the contour length. The strength of interactions between the protofilaments is described by second virial coefficient, proportional to l^2d , where l and d denote protofilament length and diameter. The resulting mature fibril consists of 2–6 protofilaments, twisted around each other. The length of the fibril is up to $10\ \mu\text{m}$, and the diameter is about 8–10 nm.^{38,39} The packing of protofilaments in the fibril is determined primarily by intrinsic physicochemical properties of the protein in terms of its amino acid sequence, charge distribution, hydrophobicity, etc., as well as by the environmental conditions.⁴⁰ At the beginning of fibril growth phase, the intertwining of the protofilaments is rare and random across the contour length. However, the number of twisting points increases with incubation time, and they tend to locate at clearly defined positions spaced by regular interval, which is called the half-pitch of the fibril (Fig. 2). This parameter linearly increases with the number and width of protofilaments. The molecular origin of fibril twist is still a matter of intensive debates.^{26,41,42} In a global sense, molecular chirality of L-amino acid residues, the main protein constituents, represents the major driving force for the observed twist. It is generally accepted that polypeptide chain composed of L-isomers of amino acids would fold either into right-handed α -helices or left-handed β -sheets.⁴³ By and large, the majority of fibrillar self-assemblies have the left-handed twist. It is worth of mentioning in this context that Gruzziel *et al.* defined the chirality of fibrillar aggregates as a dihedral angle in the filament which is connected to three consecutive vectors along the chain.⁴⁴ Furthermore, the authors distinguished two types of chirality for amyloid fibrils. Specifically, first-order chirality, determined by the imposed dihedral potential of the protofilament, was attributed to the side strand chirality. In turn, second-order chirality was ascribed to the backbone chirality, controlled by the protofilament arrangement in the fibril structure.

The key role of the inherent protein chirality in fibril growth was elegantly demonstrated by Aggeli *et al.*⁴⁵ Using a generic statistical mechanical approach, these authors showed that protein fibrillization involved the following sequence of structural transformation: Monomeric β -sheet layer \rightarrow helical tape \rightarrow twisted

ribbon (TR) (double tape) \rightarrow fibril (twisted stacks of ribbons) \rightarrow fiber (entwined fibrils). The coarse-grained description of these events relies on the representation of protein β -strand conformation as chiral rod-like unit possessing complementary groups on the opposing sides. Upper and lower faces of this rod are supposed to be chemically distinct, differing in their affinity to solvent (one side is more hydrophobic than another one). Recognition between the complementary groups on both sides initiates the association of the rod-like monomers into twisted tapes, with a twist stemming from the intrinsic chirality of naturally occurring amino acids. The tape also has facial chemical anisotropy, and different affinity of the tape faces to solvent results in a helical configuration with cylindrical curvature whose pitch (h) and radius (r) are given by

$$h = b \left(\frac{2\pi}{\gamma_0} \right) \left(1 + \left(\frac{\gamma_\nu}{\gamma_0} \right)^2 \right)^{-1}, \quad (1)$$

$$r = b \left(\frac{\gamma_\nu}{\gamma_0} \right) \left(1 + \left(\frac{\gamma_\nu}{\gamma_0} \right)^2 \right)^{-1}, \quad (2)$$

where γ_ν and γ_0 represent the bend and twist angles of the tape per monomer rod, respectively, b is the distance between two adjacent rods in the tape. Intertape attraction further gives rise to the assembly of the tapes into double tape (or twisted ribbon) configuration with identical faces on both sides, which has saddle-like (Gaussian) curvature. Subsequent stacking of the ribbons provokes the formation of fibrils, which can eventually transform into the fibrils, if fibril edges are mutually attractive. The resultant fibril width and its pitch is determined by the delicate balance between the gain in ribbon-to-ribbon attraction energy upon the stacking and the elastic cost arising from the ribbon tendency to bend and adjust its twist in response to the packing constraints imposed by the neighboring ribbons upon fibril formation.

Intertwining as a compromise between two opposing forces was also predicted by Adamcik *et al.*⁴⁶ Specifically, it was shown that twisting of the protofilaments comes from subtle interplay between the fibril elasticity and electrostatic repulsion. Twisting around the central axis represents the only way for lowering the electrostatic energy. In such a configuration, the separation distance between the charges of the same sign is increased and electrostatic repulsion is minimized. From the other hand, increased distances between the sequential segments produce the penalty in elastic energy, initiating thereby the flattered conformation of the fibril. The final periodic twist of the mature fibril is dictated by the balance between the above two processes.

However, collective results from the recent studies suggest that there exist the other possible reasons for amyloid twisting configuration implicating entropic factors⁴⁷ and hydrophobic interactions.⁴⁸ Furthermore, experimental data from the single molecule atomic force microscopy (AFM) predicted that the amyloid

periodicity is a tunable parameter, whose initial value can change upon varying ionic strength.⁴⁹ Elevating salt concentration brings about the continuous increase in the pitch value according to the equation:

$$L_2 = L_1 \left[\left(\frac{\kappa_1}{\kappa_2} \right)^{1/2} + \frac{\alpha_2}{4\pi} (\kappa_1 - \kappa_2) L_1^{3/2} \right]^{-2/3}, \quad (3)$$

where L , κ are the pitch of the fibril and Debye length, the subscript denotes salinity regime — 1 or 2 (i.e. ionic strength I_1 or I_2), α_2 is the parameter at ionic strength 2, depending on the intrinsic characteristics of the fibrils (charge density, geometry, elastic rigidity).

More general expression to relate the periodicity of the fibril to the physical properties of the constituting fibrils was derived by Assenza and co-workers.⁵⁰ Specifically, modeling the protofilament as a chain of beads with a diameter b connected by the springs with center-to-center distance $b(1 + \varepsilon)$, $\varepsilon > 0$, the half-pitch of the fibril is given by

$$Z = b(1 + \varepsilon) \frac{\pi}{A} (3n^2 - 7)^{1/2}. \quad (4)$$

Here, n is the number of protofilaments, A is a constant depending on the ionic strength of the solution, fibril elastic properties and geometrical parameters b and ε .

3. Structural Polymorphism of Fibrillary Self-Assembly

Arrangement of β -sheets within the fibril structure favors different types of intra- and inter-molecular (side chain) interactions resulting in variation of several important characteristics of protein fibrillar aggregates, such as spacing between β -sheets, nature of self-complementary regions and contact surfaces of juxtaposed protofilaments. This gives rise to the formation of a bewildering collection of polymorphs with diverse molecular architecture by the same polypeptide sequence. Current concepts of amyloid structure consider two main types of polymorphism: (i) Protofilament substructural polymorphism, and (ii) protofilament lateral assembly polymorphism.^{51,52}

Substructural polymorphism: This type of polymorphism originates from the existence of different conformations of steric zippers depending on the arrangement of the strands within the β -sheets and on the relative and packing orientation of the sheets with respect to each other and to the fibril axis.⁵³ Sawaya *et al.* postulated that steric zipper conformers may be distinguished by (i) *registration polymorphism*, i.e. relative orientation of the neighboring β -strands in the same β -sheet (parallel versus antiparallel), (ii) *facial polymorphism*, i.e. packing of β -sheets with the same (face-to-face) or different (face-to-back) surfaces adjacent to one another and (iii) *segmental polymorphism*, i.e. orientation of closely packed β -sheets in the same (up-up) or opposite (up-down) direction.³⁰ Various combinations of these steric configurations yield eight possible classes of zippers, and, consequently, eight

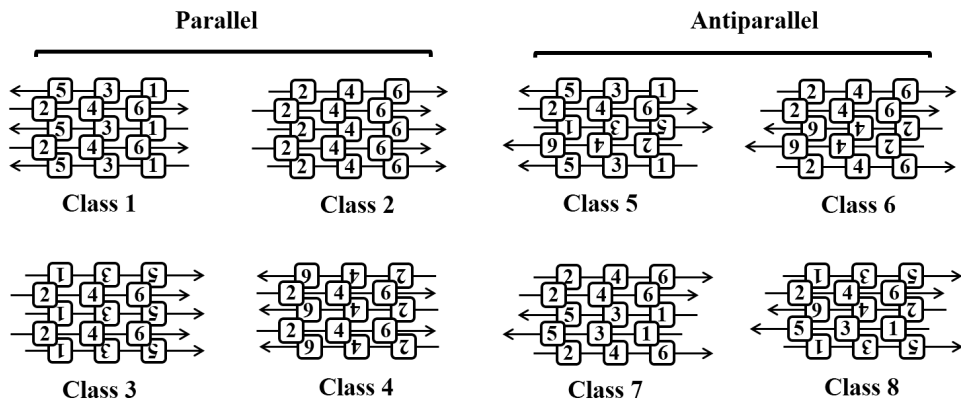


Fig. 4. Eight classes of steric zipper polymorphs. The black arrows indicate β -strand.

classes of fibril polymorphs (Fig. 4). Although this ‘eight class’ model of steric zipper conformational variation is generally accepted, recently it was theoretically demonstrated that 15 rather than 8 zipper classes can account for all allowable symmetries of homosteric zippers.⁵⁴

The analysis of all possible conformers was performed using the coordinate system in which zipper spine is oriented in such a manner that hydrogen bonds between backbone C=O and N-H groups run nearly parallel to y -axis, while its β -strands lie almost parallel to z -axis. Reasoning from all possible combinations of symmetry operations, two novel groups of steric zippers were identified, termed as head-to-head and head-to-tail. In these configurations, β -sheets run in the same or in the opposite directions along z -axis, respectively. This yields seven additional classes of steric zippers. The experimental corroboration of the amyloid spines belonging to the new classes is expected in future.

Berhanu and Masunov described the interaction between two β -sheets in zipper polymorphs from the thermodynamic viewpoint.⁵⁵ The binding energy between the sheets is given by

$$\Delta G_{\text{bind}} = \Delta G_{AB} - \Delta G_A - \Delta G_B, \quad (5)$$

where AB , A and B stand for complex (double-stranded sheet) and its components (sheet 1 and sheet 2), respectively. The free energy of AB , A and B consists of three terms:

$$\Delta G_i = E_{\text{mech}} + \Delta G_{\text{solv}} - T\Delta S, \quad (6)$$

where subscript i denotes either AB , A or B , E_{mech} is the molecular mechanics energy calculated as the sum of the internal (bonds, angles, dihedrals) (E_i), electrostatic (E_e) and van der Waals (E_{vdW}) energy

$$E_{\text{mech}} = E_i + E_e + E_{\text{vdW}}. \quad (7)$$

The term G_{solv} in Eq. (6) represents the solvation energy which can be presented as the sum of the polar and nonpolar parts:

$$\Delta G_{\text{solv}} = \Delta G_{\text{polar}} + \Delta G_{\text{nonpolar}}. \quad (8)$$

Polar term characterizes the electrostatic contribution to the solvation energy and can be calculated from the linear Poisson–Boltzmann equation, while nonpolar term is linearly dependent on the solvent accessible surface area.

Molecular dynamics simulations within the described framework allowed Berhanu and Masunov to estimate structural (inter-sheet and inter-strand distance, hydrogen bonds) and energetic parameters for different steric zipper packing polymorphs. It appeared that the polymorphs formed a given polypeptide sequence that differ in their thermodynamic stability.

Protofilament assembly polymorphism: Second class of structural polymorphism pertains to the quaternary level of fibril architecture. The common route of topological transitions displayed by a variety of amyloid-forming peptides and proteins involves the transformation from twisted ribbon to nanotube-like structures through intermediate state called helical ribbon (HR) (Fig. 5).^{56–58} Experimentally, such structural transitions have been observed for β -lactoglobulin,⁵⁹ hen egg white lysozyme,⁵⁹ apolipoprotein A-I fragments,⁶⁰ A β -peptide,⁶¹ just to name a few.

Twisted ribbons (or straight helicoids), being the precursors for the helical ribbons and nanotubes, represent the most stable configuration with nonzero Gaussian (or saddle-like) curvature, straight centerline and constant pitch, while the helical ribbons (or spiral ribbons) and nanotubes are characterized by vanishing Gaussian curvature, but significant mean curvature, helical central axis and constant tilt angle.^{26,62} Experimentally, these polymorphs are distinguished in TEM images and

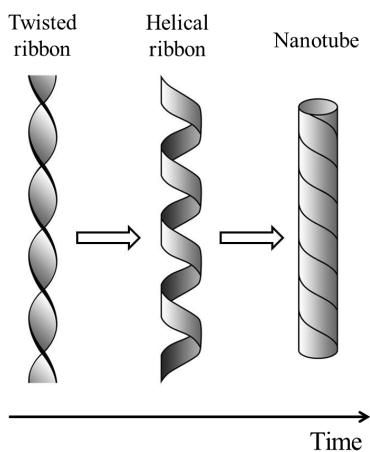


Fig. 5. Different polymorphic forms of amyloid fibrils. *Source:* The figure was reproduced from Ref. 26.






specific AFM height profiles. The physical explanation for shape selection experienced by amyloid fibrils can be made on the basis of continuum elasticity theory and differential geometry, and by considering the fibrillar aggregates as twisted nematic elastomers, a unique class of materials, formed by cross-linking liquid crystalline polymers and possessing both the high elastic properties of rubbers and orientational properties of liquid crystals.^{63,64} Specifically, it was shown that polymorphic transition arises when at least one of the mechanical elements, such as surface stress, residual strain and/or elastic modulus, is anisotropic and principle axis of curvature does not coincide with the principle geometric axis.⁶³

The presence of mechanical anisotropy gives rise to the geometric nonlinearity, which eventually drives the adoption of different conformational forms. The tunable geometrical parameters, variations in which govern the switch between different polymorphs, were identified as principal curvature, misorientation (or misalignment) angle and the ribbon width.⁶⁵ Additional factors that may affect these characteristics of a ribbon involve surface chemistry, solution pH, temperature, etc. The above considerations point to a scenario in which the competition between the out-of-plane energy contribution (responsible for the ribbon bending) and in-plane elastic energy cost (responsible for the twisting and stretching of the ribbon) underlies the final conformation of the ribbon. In the context of amyloid mechanics, width-to-thickness ratio was shown to be a key trigger of structural transition from TR to HR configuration. When this ratio is small, it is more energetically favorable for the fibril to be stretched rather than bent, and thus TR are formed. On the contrary, at large width-to-thickness ratio fibrils are easier to be bent rather than stretched, therefore HR configuration is favored.^{26,64} In other words, fibril widening reduces the relative edge energy cost per unit length, but increases substantially the energy cost of twist as a result of increased stretching energy necessary for deformation. It was shown that this delicate interplay between elastic forces and chirality gives rise to the nonmonotonic energy change as a function of fibril width. Furthermore, the transition from twisted ribbon to helical ribbon configuration occurs at the critical value of so-called Föppl–von Kármán number, defined as the dimensionless ratio of the stretching energy per unit area of the ribbon to the characteristic lateral bending energy per unit area.⁶⁶ When stretching energy is low (small values of Föppl–von Kármán number), fibril morphology corresponds to TR, while when stretching energy greatly exceeds the bending energy (high values of Föppl–von Kármán number), HR configuration becomes preferable. The main characteristics of different polymorphic forms are given in Table 1.

The dependence of polymorphic form on fibril width was corroborated by the experimental observation of time evolution of amyloid polymorphism, indicating that the formation of helical ribbons and nanotubes occurs at the latter stages of aggregation, when the width-to-thickness ratio attains large values due to increased number of protofilaments in the maturing fibril.^{61,64,67}

Seth Childers *et al.* postulated that different polymorphic forms of cross- β assemblies represent a network of paracrystalline phases (twisted ribbon phase,

Table 1. Physical characteristics of different amyloid fibril polymorphs.

	Twisted ribbon	Helical ribbon	Nanotube
Curvature	Gaussian, saddle-like	Helical	Helical
Cross-section	Rectangular		
Second moment of inertia*	$n^2 d^4 / 12$	$\frac{r_2^4 - r_1^4}{8} \sqrt{\varphi^2 - \sin^2 \varphi}$	$\left[a \left(\frac{r^2}{2} + a^2 \right) \sqrt{r^2 - a^2} + r^2 \left(\frac{r^2}{2} - 2a^2 \right) \arccos \left(\frac{a}{r} \right) \right]_{\max(a, r_1)}^{r_2}$
AFM height profile			

Note: See the text for explanation of the parameters.

helical ribbon phase, nanotube phase), arranged by their structural order in a hierarchical tree.⁶⁸

These phases are characterized by high degree of short-ranged ordering (stacks of H-bonded β -sheets) but lack three-dimensional (3D) long-range order. Likewise, the transition between TR and HR was shown to be width-dependent. Tension created by hydrogen bonding between β -strands promotes the inherent twisting of the fibrils into twisted ribbon state, while due to energy cost complementary packing of the side chains defines the helical curvature of the thick fibrils.

Based on Euler–Lagrange equations for elastic ribbon, Gerhardt-Bourke and Thamwattana described analytically the equilibrium equations for different conformations.⁶⁹ The free energy density (FED) of the elastic ribbon was shown to be:

$$F(\kappa, \tau, \alpha, \alpha') = \frac{A}{2} \kappa^2 \cos \alpha + \frac{B}{2} \kappa^2 \sin \alpha + C(\tau + \alpha' - \tau_0)^2, \quad (9)$$

where κ is the curvature of the ribbon, α is the twist angle, τ and τ_0 represent torsion and spontaneous torsion, respectively, A , B stand for bending rigidities and C denotes the torsional rigidity. The parameters A , B and C depend on elastic properties of the ribbon and geometry of its cross-section. The first derivative α' characterizes the rate of rotation of the cross-section along the centerline of the polymer chain.

The corresponding equilibrium equations of the elastic ribbon in the general case take the form:

$$\begin{aligned} \kappa \left[\alpha'' (B \cos \alpha - A \sin \alpha) - \left((\alpha')^2 - \frac{\kappa^2}{2} + \tau^2 \right) (A \cos \alpha + B \sin \alpha) \right. \\ \left. + C(\tau + \alpha' - \tau_0)(3\tau - 3\alpha' + \tau_0) \right] + \frac{4C\tau\alpha'''}{\kappa} = 0, \end{aligned} \quad (10)$$

$$-\frac{1}{\kappa} \left[2C\alpha^{(4)} + 2C\alpha'' \left(\frac{\tau^2}{\kappa} - \kappa \right) \right] + 2\tau\alpha'\kappa(B \cos \alpha - A \sin \alpha) = 0, \quad (11)$$

$$-\frac{A}{2} \kappa^2 \sin \alpha + \frac{B}{2} \kappa^2 \cos \alpha - 2C\alpha'' = 0. \quad (12)$$

The curvature of the elastic ribbon κ is generally derived from the parametric equations for the helical line. Accordingly, these equations are given by⁷⁰:

$$\begin{aligned}x &= r \cos \psi, \\y &= r \sin \psi, \\z &= h\psi,\end{aligned}\tag{13}$$

where r is the ribbon radius, ψ represents the pitch angle, $\psi \in [0, 2\pi)$, $h = r \tan \psi$ and $2\pi h$ stands for the pitch of a ribbon, P . Derivation of these equations yields the expressions for the surface curvature for twisted (κ_{TR}) and helical ribbons (κ_{HR}):

$$\begin{aligned}\kappa_{\text{TR}}(d) &= \frac{d^2}{d^2 + h^2}, \\ \kappa_{\text{HR}} &= \frac{r}{r^2 + h^2}.\end{aligned}\tag{14}$$

Here, d is the distance from the centerline of the twisted ribbon. As follows from Eq. (14), helical ribbon conformation has a constant curvature, while curvature of a twisted ribbon varies with d .

For HR fibril $B = 0$, and the resulting equilibrium equation can be written as⁶⁹

$$3Ch^2 + \frac{A}{2}(r^2 - 2h^2) - C\tau_0(r^2 + h^2)[2h + \tau_0(r^2 + h^2)] = 0.\tag{15}$$

In the case when spontaneous torsion $\tau_0 = 0$, the pitch angle can be expressed as

$$\psi = \arctan \left[\frac{1}{\sqrt{2(1 - 3C/A)}} \right].\tag{16}$$

For HR with nonzero τ_0 , the pitch angle is

$$\psi = \arctan \left[\left(\frac{1}{2 \left[2 + \frac{C}{A} \left(\frac{\tau_0}{\tau} + 3 \right) \left(\frac{\tau_0}{\tau} - 1 \right) \right]} \right)^{1/2} \right].\tag{17}$$

When ribbon adopts a TR form, vanishing torsion results in $\alpha' = \tau_0$, meaning physically that the rate of rotation is just the spontaneous torsion.

4. Elastic Properties of Amyloid Fibrils

Within the last decade along with crucial role in pathogenesis of severe disorders, amyloid fibrils were prized for their highly attractive mechanical properties such as high elasticity, stiffness (i.e. bending modulus), resistance, just to name a few.⁷¹ The origin of such superior mechanical stability lies in the strong correlation of the mechanical characteristics of amyloid fibrils with their structural parameters, including, helical periodicity, fibril length and thickness. Intermolecular forces between the stacked β -sheets promote the fibril growth up to microns in length, reaching their maximal strength in supramolecular self-assemblies, that is hardly achievable by artificial materials.^{72,73} This statement is strongly corroborated by

the results of Keten *et al.* who showed that geometrical confinement of β -sheets enhances the mechanical properties of protein crystal.⁷⁴ Hydrogen bonds are supposed to play the role of chemical glue between the layers of β -sheets, increasing thereby the mechanical stability of the protein crystal.

From the physics perspective, amyloid fibrils are considered as supramolecular semiflexible polymers, exhibiting Brownian motion in solution. Interactions with thermally excited solvent molecules result in permanent fluctuations of the polymer, which depends on its global physical properties, particularly, bending rigidity.⁷⁵ The most common approach to description of semiflexible polymers is based on the worm-like chain (WLC) model. In terms of this model, the polymer is considered as a continuous chain, whose elastic properties are determined by its bending rigidity reflecting the polymer resistance to the bending forces.^{75,76} One of the main characteristics of the polymer rigidity or flexibility is the persistence length l_p , defined as a length, at which thermal fluctuations bend the polymer chain in different directions. Another definition of l_p may be given as an arc length s along the chain, at which tangent angles become uncorrelated²⁶:

$$\langle \cos \theta(s) \rangle = \exp(-s/2l_p), \quad (18)$$

where θ is the angle between the tangent vectors to the chain at two points separated by a contour distance s . Persistence length enciphers two main characteristics of fibril rigidity, namely Young's modulus, E , and cross-sectional moment of inertia, I :

$$l_p = EI/k_B T. \quad (19)$$

E represents the intrinsic parameter of the fibril that depends mainly on the amino acid sequence of monomeric polypeptide chain. In turn, I is a geometric factor, determined by the shape and dimensions of fibril cross-section.^{26,77} These considerations point out the necessity of strict evaluation of the fibril cross-section. For the known fibril structure, cross-sectional area may be directly measured (for instance, from microscopy images), however, in most cases it represents a major challenge. Different modes of protofilament packing in the mature fibrils have been suggested to yield the accurate geometric characteristics of the fibrillar assemblies (Fig. 6). Accordingly, for the closely packed filaments, cross-sectional area is approximated as a circle of radius r , and persistence length in this case is given as²⁶

$$l_p \sim n^2 r^4 E/k_B T, \quad (20)$$

with n standing for the number of protofilaments in the fibril.

In the case of ribbon-like packing, the cross-sectional area of multistranded fibril is approximated as rectangular with the dimensions of $2r \times 2nr$, and persistence length can be written as

$$l_p \sim nr^4 E/k_B T. \quad (21)$$

Large values of cross-sectional area result in higher I and longer l_p .

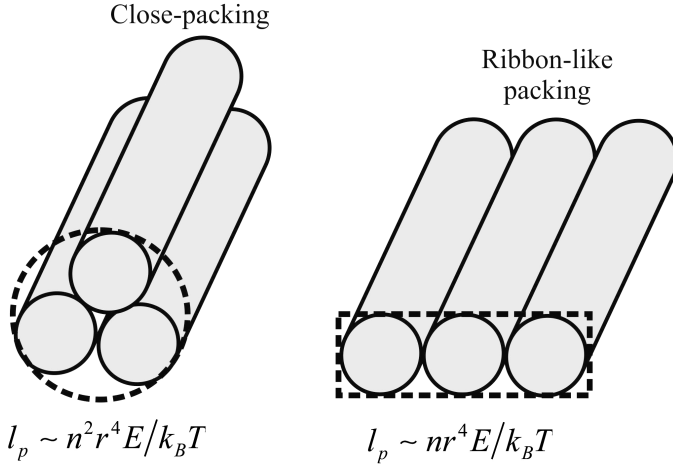


Fig. 6. Two modes of protofibril packing in the fibrillary aggregates. *Source:* The figure was reproduced from Ref. 26.

Important information can be obtained by comparing the persistence length with the contour length of the fibril L , i.e. the end-to-end distance of fully stretched polypeptide chain. If $l_p \gg L$, the polymer is considered as very rigid, while for $l_p \ll L$ the polymer appears to be extremely flexible. The polymers, whose persistence length is comparable with the contour length, $l_p \sim L$, are regarded as semiflexible.

The experimental strategies currently employed for examining the mechanics of amyloid fibrils are based mainly on the use of atomic force microscopy. Different modifications of AFM, such as nanoindentation, quantitative nanomechanical mapping, force spectroscopy, statistical analysis of shape fluctuations, etc., allow accurate determination of material properties of fibrillar aggregates.^{75,78} Using these techniques, precise estimates of amyloid mechanical strength and stiffness can be obtained. For illustrative purposes, in Table 2 we summarize the elastic characteristics of three amyloidogenic proteins, *viz.* human islet amyloid polypeptide (hIAPP), insulin and $A\beta(1-40)$ amyloid protein.⁷⁹⁻⁸¹

Table 2. Mechanical properties of protein fibrils as compared to those of some materials.

	Young's modulus (GPa)	Stiffness $N \cdot m^{-1}$	Bending rigidity $\times 10^{-26} N m^2$	Shear modulus (GPa)	Ultimate strength (GPa)	Persistence length (μm)
hIAPP	7–20	0.44–2.2	7.7–38	5.97–6.71	4–8	—
$A\beta(1-40)$	10–30	0.2–4	10–25	5.6–10.2	—	0.5–100
Insulin	3.3	0.25	9.1	0.28	0.6	22–43
Silk	1–10	0.2–4	—	—	1–1.5	—
Rubber	0.001–0.01	—	—	—	0.02–0.04	—
Steel	200	—	—	—	0.6–1.8	—

Notably, analogous parameters estimated for amyloid fibrils from other proteins and peptides are of the same order of magnitude. For the sake of comparison, we provide also some mechanical parameters of other materials. Interestingly, amyloid fibrils possess the mechanical stiffness (measured by Young's modulus) larger than that of silk, and the ultimate tensile strength comparable with that of steel. These observations suggest that protein fibrillar assemblies represent the strongest proteinaceous materials. The unique elastic properties of amyloid structure reflect the strength of intramolecular interactions of which the strongest are hydrogen bonds. Specifically, Young's modulus, that physically means the energy per unit volume, is a measure of energy density of interactions in the fibril core.⁷⁵ Since E values of amyloid reach the theoretical limits (10–30 GPa) estimated for the biomacromolecules, one may conclude that fibrillar aggregates are characterized by the highest density of hydrogen bonds available in proteins. This statement is corroborated further by Gaussian network model of amyloid fibril treating the fibril as a string of rigid monomers connected along its long axis by a Gaussian network of hydrogen bonds.⁸² This model has provided quantitative arguments of decisive role of inter-backbone hydrogen bonds in determining the material rigidity of the β -sheet aggregates.

Significant insights into the mechanics of amyloid fibrils were obtained by Yoon *et al.*⁸³ Though the study was focused on hIAPP, the conclusions drawn in the work may be extrapolated to the other amyloid-forming proteins. Speaking in more details, the main findings of this work can be formulated as follows:

- (i) *Bending rigidity of the fibril is length-dependent parameter*, i.e. there exists a critical length, above which the polymer chain becomes stable and resists mechanical bending. The threshold length is determined by the physicochemical properties and the amino acid sequence of the protein. To exemplify, for hIAPP this parameter is 70 nm, while for A β (1–43) peptide bending rigidity becomes stable at about 200 nm. The dependence of the bending rigidity on fibril length is interpreted within the framework of Timoshenko's beam theory. The analysis is based on the calculation of the total bending deflection, defined as a sum of the deflections due to bending and shear deformations. The comprehensive mathematical derivations eventually results in the expression for effective elastic bending modulus:

$$E_B = E_B^0 \left(1 + \frac{a}{b} \frac{cE_B^0 I}{G_s AL^2} \right)^{-1}, \quad (22)$$

where E_B^0 is the length-independent bending elastic modulus, G_s is intrinsic shear modulus, I , A and L stand for cross-sectional moment of inertia, cross-sectional area and length of the fibril, a and b denote the constants which depend on the boundary conditions, c is the shear coefficient, determined by cross-sectional shape.

- (ii) *Twisting configuration of the fibrillar aggregates is crucial for their mechanical properties.* Specifically, when the fibril has untwisted configuration, it is mechanically weak, and is subjected to mechanical deformations. Thus, twisting of protofilaments into the mature fibril is essential not only in providing the most thermodynamically favorable conformation, but also in determining the superior elastic characteristics of the amyloid.
- (iii) *Molecular architecture of the fibril strongly affects its mechanical properties, i.e. bending rigidity varies depending on the relative orientation of the β -sheets.* The largest values of bending rigidity correspond to the antiparallel stacking of β -sheets, while their parallel orientation results in the smallest bending rigidity. The molecular origin of this effect is supposed to lie in the so-called contact order, or the degree of native hydrogen bonding contacts. The values of this parameter for antiparallel stacking exceeds that for parallel arrangement, providing higher stiffness.

Significant role of amyloid fibril morphology in determining its mechanical properties was demonstrated also in other studies.^{77,84–86} For instance, $A\beta$ monomers of varying length were found to assemble into the fibrils with different rupture forces.^{84,85} Furthermore, modification of experimental conditions during the fibril growth was shown to yield α -synuclein aggregates with different morphologies and persistence lengths ($l_p \sim 140 \mu\text{m}$ for straight fibrils versus $l_p \sim 0.2 \mu\text{m}$ for curly fibrils).⁸⁶ Elastic behavior of different amyloid polymorphs was addressed also in the recent breakthrough paper by Usov and Mezzenga.⁷⁷ Based on Timoshenko's theory of elasticity, the authors derived the expressions for averaged second moment of inertia for three most common polymorphic states of amyloid fibrils — twisted ribbon, helical ribbon and nanotube. Within the framework of classical theory of strength of materials (theory of elasticity), amyloid aggregate in the twisted ribbon configuration is considered as a bar, or beam, with a rectangular cross-section, aligned along x -axis. The curvature radius ρ of such a bar and the bending moment M , deforming the fibril in xz -plane, are connected as

$$\frac{1}{\rho} = \frac{M}{EI_y}, \quad (23)$$

where I_y is the second moment of inertia with respect to the neutral axis y .

The energy stored in the bar is

$$U = \frac{M^2 L}{2D}. \quad (24)$$

Here, L is the length of the object, $D = EI_y$ represents the bending (flexural) rigidity. Dividing the ribbon into several segments dx , one obtains the equation for the energy stored in a segment:

$$dU = \frac{M^2 dx}{2D'(x)}. \quad (25)$$

Here, $D'(x) = EI'(x)$ with $I'(x)$ being the local second moment of inertia in the vicinity of the segment. This moment of inertia depends on the twist angle θ :

$$I'(\theta) = I_y \cos^2 \theta + I_z \sin^2 \theta - I_{yz} \sin 2\theta. \quad (26)$$

Making the necessary mathematical transformations, finally we have

$$U = \frac{M^2 L}{2E \sqrt{I_y I_z - I_{yz}^2}}, \quad (27)$$

where I_{yz} is the product moment of inertia. For twisted ribbon conformation, this parameter equals to 0. Thus, eventually:

$$U = \frac{M^2 L}{2E \sqrt{I_y I_z}}, \quad (28)$$

where $\sqrt{I_y I_z} = \langle I \rangle$ is the averaged moment of inertia. For rectangular cross-section, the area moment of inertia with respect to the principal axes y and z depends on the number of protofilaments n in the fibril and their edge size d as $I_y = n^3 d^4/12$, and $I_z = nd^4/12$, so that averaged moment of inertia for twisted ribbon is $\langle I \rangle_{\text{TR}} = n^2 d^4/12$.

Analogous derivations performed for the helical ribbon and nanotube polymorphic states yield, respectively:

$$\langle I \rangle_{\text{HR}} = \frac{r_2^4 - r_1^4}{8} \sqrt{\varphi^2 - \sin^2 \varphi}, \quad (29)$$

$$\langle I \rangle_{\text{tube}} = \left[a \left(\frac{r^2}{2} + a^2 \right) \sqrt{r^2 - a^2} + r^2 \left(\frac{r^2}{2} - 2a^2 \right) \arccos \left(\frac{a}{r} \right) \right]_{\max(a, r_1)}^{r_2}, \quad (30)$$

where r_1 and r_2 stand for the inner and outer radii of the fibril, φ is the segment angle and a represents the shift of the neutral axis from the central axis (this parameter reflects the asymmetry of contributions to the total stored energy arising from compression and adhesion). Though the derived equations are based on some approximations and assumptions, they nevertheless highlight the important contribution of structure-property relationship into the nanomechanics of amyloid.

5. Liquid Crystalline Phase Behavior of Amyloids: Isotropic–Nematic Transition

Colloidal nature of amyloid fibrils implies that these systems are characterized by a complex liquid crystalline behavior. Indeed, protein fibrillar aggregates were shown to undergo isotropic–nematic (I–N) transition in water under the conditions of low volume fractions.³⁷ At low densities, protein fibrils are randomly distributed in solution due to the dominating contribution of orientational entropy to the free energy of the system. However, when the concentration is far above critical value (critical fibrillar concentration), the major impact belongs to the packing entropy due to increased frequency of fibril collisions (excluded volume effect).

This results in the transition of liquid crystals into the nematic phase, in which translational entropy favors parallel alignment of the fibrils since such arrangement minimizes the excluded volume effect. I–N transition is generally rationalized within the framework of Onsager’s theory developed for the prediction of phase behavior of anisotropic particles.⁸⁷ Accordingly, for suspensions of uncharged monodisperse rigid rods with length L and diameter D , which are involved in the hard-core interactions, I–N transition occurs at the volume fraction⁸⁹:

$$\phi_{\text{IN}} = 4 \frac{D}{L}. \quad (31)$$

This equation yields the so-called “bifurcation point”, i.e. the point of coexistence of two phases. Further increase in particle concentration results in purely nematic phase.

If the particles bear the charge, to account for the electrostatic repulsion between the particles and their surrounding layers, diameter D in Eq. (31) is replaced by the effective diameter D_{eff} :

$$D_{\text{eff}} = D + \kappa^{-1} \left(\ln A + C + \ln 2 - \frac{1}{2} \right), \quad (32)$$

where κ^{-1} is the Debye length, $C = 0.577$ is the Euler’s constant, A is given by

$$A = 2\pi\nu_{\text{eff}}^2 \kappa^{-1} Q \exp(-\kappa D), \quad (33)$$

where ν_{eff} is the linear charge density of the rod (i.e. the number of charges per unit length), Q is the Bjerrum length ($Q = 0.712 \text{ nm}$ for water at room temperature).

Based on Onsager theory, isotropic–nematic transition is defined by means of dimensionless constant c , determining the strength of interactions between the fibrils²⁶:

$$c = B_2^{\text{iso}} \rho. \quad (34)$$

Here, $B_2^{\text{iso}} = (\pi/4)D_{\text{eff}}L^2$ is the second virial coefficient, $\rho = N/V$ is the number density of N fibrils dispersed in volume V . Assembling all the above expressions, one finally obtains the general expression for fibril volume fraction at which I–N transition takes place:

$$\phi_{\text{IN}} = c^* \frac{D^2}{D_{\text{eff}}L}. \quad (35)$$

Using this approach Bolisetty *et al.* succeeded in obtaining the phase diagram plot for β -lactoglobulin amyloid fibrils as a function of protein concentration, pH and ionic strength.⁸⁸ The main result reached is that increasing pH and ionic strength give rise to the delay in I–N transition due to reduced Debye length and D_{eff} .

Analogous conclusion has been drawn by Li who proposed a toy thermodynamic model for analyzing the isotropic–nematic transition.⁸⁹ By combining the statements from the models for nematic ordering of linear structures and charged

rods, with the models of amyloid elasticity, Li derived the expressions for FED of isotropic

$$f_I = (\chi S_I^2 + 2S_I)e^{-\xi} + \frac{\pi D_{\text{eff}} \zeta^2 c_I^2}{4}, \quad (36)$$

$$f_N = -\frac{4\lambda^*}{P} \left[\left(\chi - \frac{\zeta}{4\lambda^*} \right) S_N^2 + 2S_N \right] e^{-\xi} + D_{\text{eff}} \zeta^2 \sqrt{\frac{\pi\lambda^*}{P}} c_N^2, \quad (37)$$

where χ is the energy strength, $S_{I,N}$ and $c_{I,N}$ are the average aggregation numbers and protein volume fractions in I and N phases, respectively, ξ and ζ denote the binding energy and the fibril length per monomer, respectively, P is the persistence length of the fibril and λ^* is the fibril depletion length. At the co-existence of two phases, the total FED is given by

$$f_{\text{tot}}(c_I, c_N) = v_I f_I(c_I) + v_N f_N(c_N), \quad (38)$$

where $v_{I,N}$ mean the proportion of isotropic or nematic component in the system, respectively. Since $v_I = (c_N - c_{\text{tot}})/(c_N - c_I)s$ and $v_N = (c_{\text{tot}} - c_I)/(c_N - c_I)$, the proportion of the isotropic/nematic components may be obtained by minimizing the total FED with respect to c_I and c_N . Application of this formalism to analysis of nematic ordering of fibrils from hen egg white lysozyme showed that the lower and upper concentrations for phase separation are ~ 0.65 and 1.05 mM, respectively.

6. Concluding Remarks

In the present contribution, we made an attempt to structurize the existing knowledge of amyloid fibrils from the polymer physics standpoint. Being the product of protein misfolding, fibrillar aggregates represent highly ordered semiflexible polymers exhibiting extremely attractive mesoscopic properties which can be tuned both by intrinsic physicochemical characteristics of polypeptide chain and milieu conditions. High mechanical rigidity and stability in couple with chiral, polar and charged nature of amyloids provide them with unique physical properties in one, two and even three dimensions. The tandem of amyloid biological origin and its superior nanomechanics renders protein fibrils attractive candidates for artificial materials with a diversity of beneficial biological, medical and technological applications. For disease-related amyloids, deeper understanding of fibril characteristics may shed light on the pathogenesis and molecular mechanisms of the disorders, as well as on the strategies of amyloidosis prevention at atomistic level. In the context of nanotechnology and functional material science, knowing the physical properties of protein fibrillar aggregates is crucially required for the design of novel nanomaterials with unprecedented qualities.

Acknowledgments

The author is sincerely grateful to Prof. Galyna Gorbenko for helpful discussions on the topic of the manuscript.

References

1. R. S. Harrison, P. C. Sharpe, Y. Singh and D. P. Fairlie, *Rev. Physiol. Biochem. Pharmacol.* **159**, 1 (2007).
2. F. Chiti and C. M. Dobson, *Ann. Rev. Biochem.* **75**, 333 (2006).
3. R. Tycko, *Annu. Rev. Phys. Chem.* **62**, 279 (2011).
4. J. D. Sipe and A. S. Cohen, *J. Struct. Biol.* **130**, 88 (2000).
5. A. J. Howie, D. B. Brewer, D. Howell and A. P. Jones, *Lab. Invest.* **88**, 232 (2008).
6. S. L. Gras, L. J. Waddington and K. N. Goldie, *Methods Mol. Biol.* **752**, 197 (2011).
7. K. L. Morris and L. C. Serpell, *Methods Mol. Biol.* **849**, 121 (2012).
8. M. Sunde, L. C. Serpell, M. Bartlam, P. E. Fraser, M. B. Pepys and C. C. F. Blake, *J. Mol. Biol.* **273**, 729 (1997).
9. W. Wei, X. Wang and J. W. Kusiak, *J. Biol. Chem.* **277**, 17649 (2002).
10. A. J. Bruce, B. Malfroy and M. Baudry, *Proc. Natl. Acad. Sci. USA* **93**, 2312 (1996).
11. H. B. Nygaard and S. M. Strittmatter, *Arch. Neurol.* **66**, 1325 (2009).
12. Y. Verdier, M. Zarandi and B. Penke, *J. Pept. Sci.* **10**, 229 (2004).
13. P. Walsh, G. Vanderlee, J. Yau, J. Campeau, V. L. Sim, C. M. Yip and S. Sharpe, *J. Biol. Chem.* **289**, 10419 (2014).
14. P. Cao, A. Abedini, H. Wang, L. H. Tu, X. Zhang, A. M. Schmidt and D. Raleigh, *Proc. Natl. Acad. Sci. USA* **110**, 19279 (2013).
15. P. Tian, W. Boomsma, Y. Wang, D. Otzen, M. Jensen and K. Lindorff-Larsen, *J. Am. Chem. Soc.* **137**, 22 (2015).
16. C. L. L. Pham, A. H. Kwan and M. Sunde, *Essays Biochem.* **56**, 207 (2014).
17. R. P. McGlinchey, F. Shewmaker, K. Hu, P. McPhie, R. Tycko and R. Wickner, *J. Biol. Chem.* **286**, 8385 (2011).
18. M. R. Champan, L. S. Robinson, J. S. Pinkner, R. Roth, J. Heuser, M. Hammar, S. Normark and S. J. Hultgren, *Science* **295**, 851 (2007).
19. D. M. Fowler, A. V. Koulov, C. Alory-Jost, M. S. Marks, W. E. Balch and J. W. Kelly, *PLoS Biol.* **4**, e6 (2006).
20. A. Mostaert, R. Crockett, G. Kearns, I. Cherny, E. Gazit, L. C. Serpell and S. Jarvis, *Arch. Histol. Cytol.* **72**, 199 (2009).
21. S. K. Maji, M. H. Perrin, M. R. Sawaya, S. Jessberger, K. Vadodaria, R. A. Rissman, P. S. Singru, K. P. Nilsson, R. Simon, D. Schubert, D. Eisenberg, J. Rivier, P. Sawchenko, W. Vale and R. Riek, *Science* **325**, 328 (2009).
22. S. Maji, D. Schubert, C. Rivier, S. Lee, J. Rivier and R. Riek, *PLoS Biol.* **6**, e17 (2008).
23. S. Mankar, A. Anoop, S. Sen and S. Maji, *Nano Rev.* **2**, 6032 (2011).
24. T. Scheibel, R. Parthasarathy, G. Sawicki, X. Lin, H. Jaeger and S. Lindquist, *Proc. Natl. Acad. Sci. USA* **100**, 4527 (2003).
25. M. Reches and E. Gazit, *Science* **300**, 625 (2003).
26. J. Adamcik and R. Mezzenga, *Macromolecules* **45**, 1137 (2012).
27. M. Schleegeer, C. C. vandenAkker, T. Deckert-Gaudig, V. Deckert, K. Velikov, G. Koenderink and M. Bonn, *Polymer* **54**, 2473 (2013).
28. O. Makin and L. Serpell, *FEBS J.* **272**, 5950 (2005).
29. L. Serpell, M. Sunde, M. Benson, G. Tennent, M. Pepys and P. Fraser, *J. Mol. Biol.* **300**, 1033 (2000).
30. M. R. Sawaya, S. Sambashivan, R. Nelson, M. I. Ivanova, S. A. Sievers, M. I. Apolstol, M. J. Thompson, M. Balbirnie, J. J. Wiltzius, H. T. McFarlane, A. O. Madsen, C. Riek and D. Eisenberg, *Nature* **447**, 453 (2007).
31. L. Vitagliano, F. Stanzione, A. De Simone and L. Esposito, *Biopolym.* **91**, 1161 (2009).
32. P. Arosio, T. Knowles and S. Linse, *Phys. Chem. Chem. Phys.* **17**, 7606 (2015).

33. S. Cohen, S. Linse, L. Luheshi, E. Hellstrand, D. White, L. Rajah, D. Otzen, M. Vendruscolo, C. Dobson and T. Knowles, *Proc. Natl. Acad. Sci. USA* **110**, 9758 (2013).
34. K. Eden, R. Morris, J. Gilliam, C. MacPhee and R. Allen, *Biophys. J.* **108**, 632 (2015).
35. P. Arosio, R. Cukalevski, B. Frohm, T. Knowles and S. Linse, *J. Am. Chem. Soc.* **136**, 219 (2014).
36. S. Bolisetty, J. Adamcik and R. Mezzenga, *Soft Mat.* **7**, 493 (2011).
37. J. Jung and R. Mezzenga, *Langmuir* **26**, 504 (2010).
38. A. Rellini, R. Rolandi, M. Bolognesi, M. Aboudan, G. Merlini, V. Bellotti and A. Gliozzi, *Biochim. Biophys. Acta* **1690**, 33 (2004).
39. R. Khurana, C. Ionescu-Zanetti, M. Pope, J. Li, L. Nelson, M. Ramirez-Alvarado, L. Regan, A. Fink and S. Carter, *Biophys. J.* **85**, 1135 (2003).
40. G. Gorbenko and P. K. J. Kinnunen, *Chem. Phys. Lipids* **141**, 72 (2006).
41. W. Dzwolak, *Chirality* **26**, 580 (2014).
42. L. R. Volpatti, M. Vendruscolo, C. M. Dobson and T. Knowles, *ACS Nano* **7**, 10443 (2013).
43. W. Dzwolak and M. Pecul, *FEBS Lett.* **579**, 6601 (2005).
44. M. Gruziel, W. Dzwolak and P. Szymczak, *Soft Mat.* **9**, 8005 (2013).
45. A. Aggeli, I. Nyrkova, M. Bell, R. Harding, L. Carrick, T. McLeish, A. Semenov and N. Boden, *Proc. Natl. Acad. Sci. USA* **98**, 11857 (2001).
46. J. Adamcik, J. Jung, J. Flakowski, P. De Los Rios, G. Dietler and R. Mezzenga, *Nat. Nanotechnol.* **5**, 423 (2010).
47. I. Shamovsky, G. Ross and R. Riopelle, *J. Phys. Chem. B* **104**, 11296 (2000).
48. J. van Gestel and S. de Leeuw, *Biophys. J.* **92**, 1157 (2007).
49. J. Adamcik and R. Mezzenga, *Soft Mat.* **7**, 5437 (2011).
50. S. Assenza, J. Adamcik, R. Mezzenga and P. De Los Rios, *Phys. Rev. Lett.* **113**, 268103 (2014).
51. L. Kreplak and U. Aebi, *Adv. Protein Chem.* **73**, 217 (2006).
52. Y. Miller, B. Ma and R. Nussimov, *Chem. Rev.* **110**, 4820 (2010).
53. J. Wiltzius, M. Landau, R. Nelson, M. Sawaya, M. Apostol, L. Goldschmidt, A. Soriaga, D. Cascio, K. Rajashankar and D. Eisenberg, *Nat. Struct. Mol. Biol.* **16**, 973 (2009).
54. J. Stroud, *Acta Crystallogr. D* **69**, 540 (2013).
55. W. Berhanu and A. Masunov, *Peptide Sci.* **98**, 131 (2011).
56. J. Juarez, P. Taboada and V. Mosquera, *Biophys. J.* **96**, 2353 (2009).
57. I. Usov, J. Adamcik and R. Mezzenga, *Faraday Discuss.* **166**, 151 (2013).
58. S. Zhang, M. Andreasen, J. Nielsen, L. Liu, J. Song, G. Ji, F. Sun, T. Skrydstrup, F. Besenbacher, N. Nielsen, D. Otzen and M. Dong, *Proc. Natl. Acad. Sci. USA* **110**, 2798 (2013).
59. C. Lara, J. Adamcik, S. Jordens and R. Mezzenga, *Biomacromolecules* **12**, 1868 (2011).
60. M. Giryh, G. Gorbenko, V. Trusova, E. Adachi, C. Mizuguchi, K. Nagao, H. Kawashima, K. Akaji, S. Lund-Katz, M. Philips and H. Saito, *J. Struct. Biol.* **185**, 16 (2014).
61. J. Adamcik, V. Castelletto, S. Bolisetty, I. Hamley and R. Mezzenga, *Angew. Chem., Int. Ed.* **50**, 5495 (2011).
62. J. Adamcik and R. Mezzenga, *Curr. Opin. Colloid Interface Sci.* **17**, 369 (2012).
63. L. Teresi and V. Varano, *Soft Mat.* **9**, 3081 (2013).
64. Y. Sawa, F. Ye, K. Urayama, T. Takigawa, V. Gimenez-Pinto, R. Selinger and J. Selinger, *Proc. Natl. Acad. Sci. USA* **108**, 6364 (2011).
65. Z. Chen, C. Majidi, D. Srolovitz and M. Haataja, *Appl. Phys. Lett.* **98**, 011906 (2011).

66. R. Ghafouri and R. Bruinsma, *Phys. Rev. Lett.* **94**, 138101 (2005).
67. E. Pashuck and S. Stupp, *J. Am. Chem. Soc.* **132**, 8819 (2010).
68. W. Seth Childers, N. Anthony, A. Mehta, K. Berland and D. Lynn, *Langmuir* **28**, 6386 (2012).
69. A. Gerhardt-Bourke and N. Thamwattana, *Phys. Rev. E* **87**, 046601 (2013).
70. A. Pressley, *Elementary Differential Geometry*, (Springer-Verlag, 2001).
71. T. Knowles and M. Buehler, *Nat. Nanotechnol.* **6**, 469 (2011).
72. G. Yoon, Y. Kim, K. Eom and S. Na, *Appl. Phys. Lett.* **102**, 011914 (2013).
73. D. Ganchev, N. Cobb, K. Surewicz and W. Surewicz, *Biophys. J.* **95**, 2909 (2008).
74. S. Ketten, Z. Xu, B. Ihle and M. Buehler, *Nature Mater.* **9**, 359 (2010).
75. L. Volpatti and T. Knowles, *J. Polym. Sci. B* **52**, 281 (2014).
76. T. Witte, L. Haller, E. Luttmann, J. Krüger, G. Fels and K. Huber, *J. Struct. Biol.* **159**, 71 (2007).
77. I. Usov and R. Mezzenga, *ACS Nano* **8**, 11035 (2014).
78. T. Fukuma, A. Mostaert and S. Jarvis, *Tribol. Lett.* **22**, 233 (2006).
79. J. Smith, T. Knowles, C. Dobson, C. MacPhee and M. Welland, *Proc. Natl. Acad. Sci. USA* **103**, 15806 (2006).
80. B. Choi, G. Yoon, S. Lee and K. Eom, *Phys. Chem. Chem. Phys.* **17**, 1379 (2015).
81. M. Solar and M. Buehler, *Nanoscale* **4**, 1177 (2012).
82. T. Knowles, A. Fitzpatrick, S. Meehan, H. Mott, M. Vendruscolo, C. Dobson and M. Welland, *Science* **318**, 1900 (2007).
83. G. Yoon, J. Kwak, J. Kim, S. Na and K. Eom, *Adv. Funct. Mater.* **21**, 3454 (2011).
84. A. Karsai, Z. Martonfalvi, A. Nagy, L. Grama, B. Penke and M. Kellermayer, *J. Struct. Biol.* **155**, 316 (2006).
85. M. Kellermayer, L. Grama, A. Karsai, A. Nagy, A. Kahn, Z. Datki and B. Penke, *J. Biol. Chem.* **280**, 8464 (2005).
86. G. Bhak, S. Lee, J. Park, S. Cho and S. Paik, *Biomaterials* **31**, 5986 (2010).
87. L. Onsager, *Annu. N. Y. Acad. Sci.* **51**, 627 (1949).
88. S. Bolisetty, L. Harnau, J. Jung and R. Mezzenga, *Biomacromolecules* **13**, 3241 (2012).
89. C. F. Li, *Phys. Rev. E* **80**, 031902 (2009).